

RESEARCH ARTICLE | FEBRUARY 12 2024

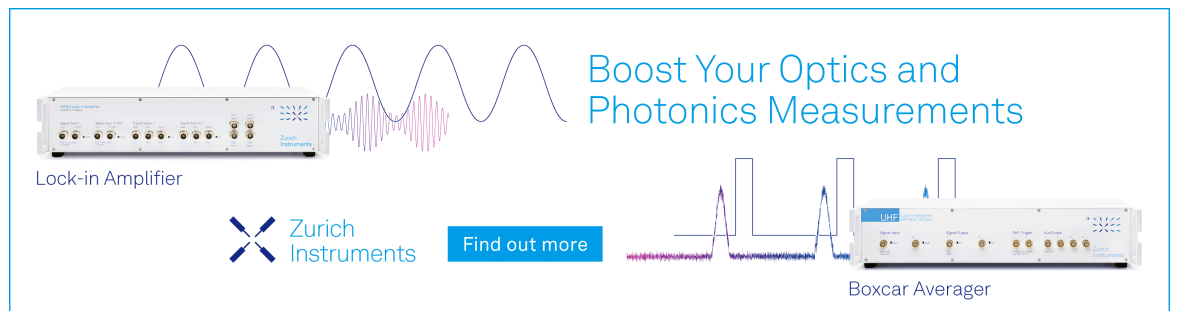
Spectroscopic observation of Feshbach resonances in the tellurium dimer anion

Shuaiting Yan ; Rui Zhang ; Yuzhu Lu; Chuangang Ning  




J. Chem. Phys. 160, 064303 (2024)

<https://doi.org/10.1063/5.0190983>



Boost Your Optics and Photonics Measurements

Lock-in Amplifier

 Zurich Instruments

[Find out more](#)

Boxcar Averager

Spectroscopic observation of Feshbach resonances in the tellurium dimer anion

Cite as: J. Chem. Phys. 160, 064303 (2024); doi: 10.1063/5.0190983

Submitted: 10 December 2023 • Accepted: 15 January 2024 •

Published Online: 12 February 2024



View Online



Export Citation



CrossMark

Shuaiting Yan,  Rui Zhang,  Yuzhu Lu, and Chuangang Ning^{a)} 

AFFILIATIONS

Department of Physics, State Key Laboratory of Low Dimensional Quantum Physics, Frontier Science Center for Quantum Information, Tsinghua University, Beijing 100084, China

^{a)} Author to whom correspondence should be addressed: ningcg@tsinghua.edu.cn

ABSTRACT

We report on the high-resolution photodetachment spectroscopy of the cryogenically cooled anionic tellurium dimer (Te_2^-). The high-resolution resonant photoelectron spectrum yields an accurate electron affinity of $16\,689.7(92)\text{ cm}^{-1}$ or $2.0693(11)\text{ eV}$ for Te_2 . Two resonant states of Te_2^- anions have been identified, positioned at $1092(17)\text{ cm}^{-1}$ below and $250(11)\text{ cm}^{-1}$ above the photodetachment threshold, respectively. The spectra of resonant two-photon detachment (R2PD) and autodetachment from a specific vibrational level through a Feshbach resonance exhibit notable non-Franck-Condon behaviors. Using the spectroscopic data from the current experiment, the equilibrium bond distances and spectroscopic constants of the ground state and two electronically excited states of Te_2^- were determined.

Published under an exclusive license by AIP Publishing. <https://doi.org/10.1063/5.0190983>

I. INTRODUCTION

The electronic configuration of main group VIA elements (O-Te) is ns^2np^4 . Their diatomic molecules typically exhibit many complicated electronic states due to the six valence electrons, coupled with active chemical properties.¹⁻⁸ Among these species, the tellurium dimer possesses significantly relativistic effects and strong spin-orbit coupling effects, contributing to further complicated spectra.⁹⁻¹¹ Thus, the spectroscopic characteristics of the tellurium dimer have attracted the attention of researchers.¹²⁻¹⁵ As early as 1940, the internuclear distance of the gas molecules Te_2 was measured to be $2.59 \pm 0.02\text{ \AA}$ via the electron diffraction photograph.¹⁶ Berkowitz obtained the ionization potential of Te_2 ($8.29 \pm 0.03\text{ eV}$) and the dissociation energy of Te_2 [$D_0(\text{Te}_2) = 62.3\text{ kcal/mol}$] from the photoionization-efficiency curve for the first time. Meanwhile, the splitting value between the 0_g^+ state and the 1_g state of the Te_2 ground electronic state (${}^3\Sigma_g^-$) was determined to be $0.35 \pm 0.04\text{ eV}$.¹⁷ However, Yee *et al.* observed a detailed vibrational and rotational absorption spectrum of the A $0_u^+ - X\ 0_g^+$ and B $0_u^+ - X\ 0_g^+$ bands of gaseous Te_2 using the Ar^+ laser, and they believed that the ground state X $1_g - X\ 0_g^+$ splitting value is within 2230 cm^{-1} .¹⁸ Then, Barrow and Yee¹⁹ and Li *et al.*²⁰ also observed the zero-field splitting [$X_1\ ({}^3\Sigma_g^-, 0_g^+) \sim X_2\ ({}^3\Sigma_g^-, 1_g)$] in the ground state of

the diatomic molecule Te_2 through spectroscopic experiments. Furthermore, Berkowitz investigated the ionization energies of seven electronic states of Te_2 ($X^2\Pi_{g,1/2}$, ${}^2\Pi_{g,3/2}$, $a^4\Pi_u$, $A^2\Pi_u$, $b^4\Sigma_g^-$, $B^2\Sigma_g^-$, and $c^4\Sigma_u^-$ states) using the photoelectron energy spectroscopy.²¹ Meanwhile, Stone and Barrow first discovered a new transition band attributed to B $1_u - X\ 1_g$ by analyzing the laser excited fluorescence spectra of gaseous Te_2 and gave detailed spectroscopic constants for the ground state of ${}^{130}\text{Te}_2$.²² The vibrationally well resolved spectrum of Te_2 in rare gas matrices was also investigated by laser-induced fluorescence techniques, suggesting that its spectroscopic constants were minimally perturbed by the solid medium.²³ At the same time, Effantin *et al.* recorded laser-induced fluorescence bands of Te_2 by Fourier transform spectrometry in the range $5900\text{--}15\,000\text{ cm}^{-1}$ with the 4067 \AA line of the krypton-ion laser and identified a new electronic state ($b\ 1\Sigma_g^+$) above the ground state (${}^3\Sigma_g^-, 0_g^+$) by 9600.2 cm^{-1} .²⁴ In addition, Bowen group recorded the photoelectron spectrum of Te_2^- and measured the electron affinity of Te_2 to be $1.92 \pm 0.07\text{ eV}$.²⁵ David investigated the magnetic moment of Te_2 molecule by the Stern-Gerlach magnetic deflection method.²⁶ Besides the diatomic Te_2 molecule, experimental investigations of small tellurium clusters have been reported.²⁷ Duncan group produced the tellurium clusters in the size range of 2–20 atoms through laser vaporization and simultaneously obtained mass-selected

photodissociation spectra using an ultraviolet laser.²⁸ Analogously, isolated tellurium clusters Te_n ($n = 2-9$) were generated in a supersonic molecular beam and their vacuum-UV-photoelectron spectra were measured at a photo energy of $h\nu = 8.3$ eV via a photoionization-photoelectron-photoion triple coincidence method, revealing that the spectra of the odd-membered tellurium clusters have a tendency to be split and broadened, in contrast to those of the even-membered clusters.²⁹

Corresponding to the aforementioned experimental studies, theoretical research studies on the diatomic molecule Te_2 have also been conducted.³⁰⁻³² For example, Balasubramanian and Ravimohan carried out complete active space MCSCF(CASSCF)/first-order configuration interaction (FOCI) calculations on 22 electronic states of Te_2 . They corrected and predicted the properties of a number of electronic states observed or unobserved in previous experiments.³³ Next, Ferber and collaborators developed a quasi-relativistic method of *ab initio* calculations on molecular excited states and electronic transition moments within the relativistic effective potential approximation. They applied this method to calculate the radiative lifetime of low-lying rovibrational levels of the $\text{A}0_u^+$, $\text{B}0_u^+$, and $\text{B}1_u$ states of $^{130}\text{Te}_2$.³⁴ A new atomic natural orbital type basis set including high angular momentum functions up to $l = 6$ was constructed for tellurium. Employing this set in combination with the multi-reference configuration interaction (MRCI) method, the potential curves and spectroscopic constants of the ground and excited states of Te_2^{-0} were predicted.³⁵

Although there are extensive studies on the Te_2 molecule, no high-resolution spectroscopic research of anionic tellurium dimer has been reported. In the current work, we investigated the resonant photoelectron spectroscopy of a cryogenically cooled Te_2^- anion utilizing the high-resolution slow-electron velocity-map imaging (SEVI) method.³⁶⁻⁴¹

II. EXPERIMENTAL AND THEORETICAL METHODS

The experiments were conducted on a home-built apparatus, a slow photoelectron velocity-map imaging spectrometer equipped with a cryogenically cold ion trap (cryo-SEVI). The details of our spectrometer can be found elsewhere.⁴²⁻⁴⁵ Briefly, Te_2^- anions were generated in a laser vaporization source by the laser ablation of a rotating and translating arsenic telluride target with the second harmonic (532 nm) light pulse of an Nd:YAG laser (Continuum Surelite II-10). The produced tellurium dimer anions were carried by the helium gas with a background pressure of ~ 0.3 MPa. Negatively charged clusters were guided into the radio frequency (RF) ion trap by a hexapole ion guide and then cooled through collisions with the buffer gas ($\text{He}:\text{H}_2 = 4:1$) in the trap. The temperature of the ion trap was maintained at 15 K. The trapped anions were cooled down to their ground vibrational and electronic states after sufficient collisions. Following a cooling period of 45 ms, the anions were ejected from the cold trap into an orthogonal Wiley-McLaren type time-of-flight (TOF) mass spectrometer.⁴⁶ The Te_2^- anions with $m = 260$ were selectively filtered with a mass gate, were focused into the interaction region of velocity map imaging (VMI), and were then photodetached by a tunable laser from the signal light of an optical parametrical oscillator (OPO, 405–709 nm, linewidth ~ 6 cm^{-1}) pumped using a Quanta-Ray Lab 190 Nd:YAG laser operating at 20 Hz. The photodetached electrons were projected onto

a 2D position-sensitive detector via a set of electrostatic lens and recorded using a charge-coupled device (CCD) camera.⁴⁷ Since the distribution of outgoing photoelectrons exhibits a cylindrical symmetry,⁴⁴ the maximum entropy velocity Legendre reconstruction (MEVELER) method was used to reconstruct the 3D photoelectron distribution from the projected 2D image,^{48,49} yielding the electron energy distribution. The spectrometer was calibrated using the known spectra of $^{130}\text{Te}^-$.⁴⁵ The energy resolution of our cryo-SEVI spectrometer is better than 0.1 meV near the photodetachment threshold.⁵⁰

To investigate the resonance, the spectrometer can be changed from the standard SEVI mode to the scanning mode.⁵¹ In the scanning mode, the photoelectron signals and the residual Te_2^- anions were both recorded using a high-speed oscilloscope connected to the phosphor screen due to their different arrival time on the phosphor screen. We acquired the positions of resonance peaks via monitoring the ratio of the photoelectron signal intensity to the residual anion beam intensity as a function of the wavelength of the photodetachment laser. Each data point was an accumulated result of 50 laser shots.

To interpret the observed spectra, we also conducted multi-reference configuration interaction (MRCI) calculations using the Molpro software package.⁵² The spin-orbit coupling has been included in the calculations. The correlation consistent basis set aug-cc-pVQZ-PP for Te with the ECP28MDF pseudopotential was used.⁵³⁻⁵⁶

III. RESULTS AND DISCUSSION

A. High-resolution photoelectron spectra and Franck-Condon analysis

Figure 1(a) displays the photoelectron image and the binding energy spectrum at the wavelength of 480 nm. In the present work, vibrational hot bands are eliminated due to the ion trap kept at a low temperature of 15 K, leading to a significantly improved photoelectron spectra resolution. The spectrum contains two prominent electronic bands (X_1 and X_2). Based on the known electronic structure of Te_2 from the NIST database,⁵⁷ peaks X_1 and X_2 can be assigned as transitions from the anion ground state $^2\Pi_{3/2}$ to the two splitting states (0_g^+ , 1_g) of the neutral ground state $^3\Sigma_g^-$.^{9,22,23,35} The two electronic bands contain a series of approximately equally spaced peaks, which are the vibrational progression of the Te-Te stretching. For these peaks, we use 0 and $0'$ to label the transition from the ground vibrational level of the ground electronic state of Te_2^- [$^2\Pi_{3/2}$] to that of the two splitting states (0_g^+ , 1_g) of the neutral ground state ($^3\Sigma_g^-$), respectively. Transitions to the respective vibrational excited states of the two splitting states of Te_2 are represented by ν , $\nu' = 1-5$. The gap between the 0 and $0'$ peaks is determined to be $1980(16)$ cm^{-1} in the current work, which is in reasonable agreement with the value obtained from the NIST database (1974.9 cm^{-1})^{22,23} and our theoretically predicted gap (1918 cm^{-1}) via multi-reference configuration interaction (MRCI) calculations using the Molpro software package.⁵²

It is noteworthy that the weak band preceding peak 0 in Fig. 1 is attributed to the $^2\Pi_{1/2}$ state of Te_2^- . The $^2\Pi_{1/2}$ state is a metastable state since it cannot decay into the ground state $^2\Pi_{3/2}$ via an electronic dipole transition. We observed that the buffer gas collisions

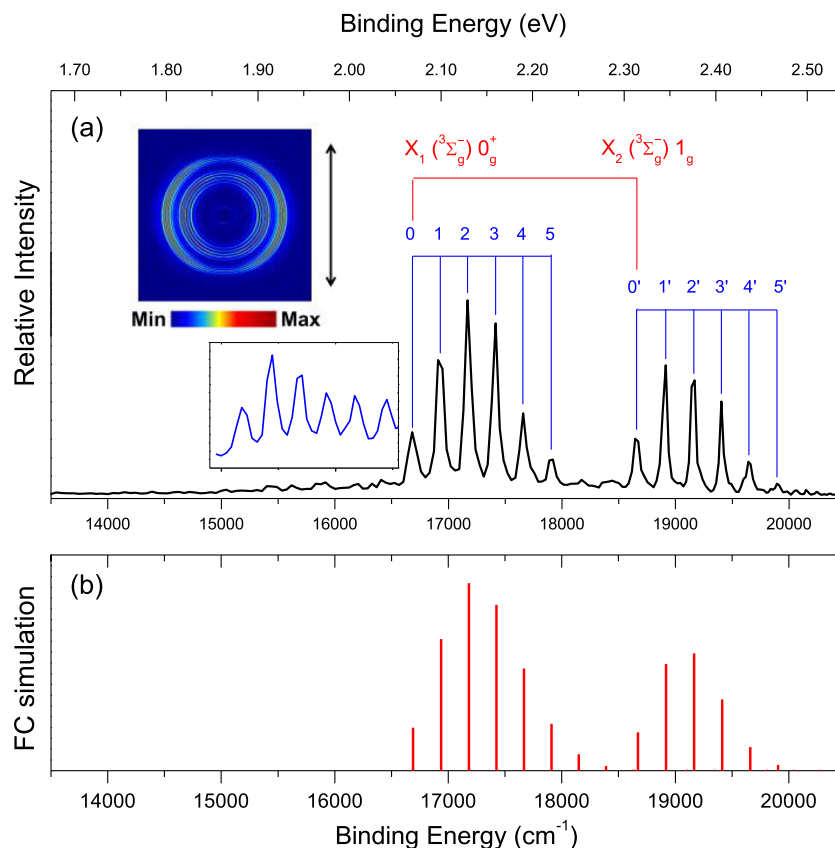


FIG. 1. (a) Non-resonant photoelectron spectrum and image of Te_2^- at 480 nm. The double arrow indicates the polarization of the photodetachment laser. Two main electronic bands from the Te_2^- ground state are band X_1 [$(^3\Sigma_g^-) 0_g^+ \leftarrow ^2\Pi_{3/2}$] and band X_2 [$(^3\Sigma_g^-) 1_g \leftarrow ^2\Pi_{3/2}$]. The vibrational quantum number of the final states is marked on the top. The inset shows a series of peaks from a metastable state $^2\Pi_{1/2}$ to $(^3\Sigma_g^-) 0_g^+$, which was obtained under a different condition. (b) The red vertical lines are from the Franck-Condon simulation.

in the cold ion trap cannot efficiently quench this excited either. Its intensity depends on the laser ablation ion source conditions and the buffer gas density in the ion trap. It is challenging to obtain a stable signal of $^2\Pi_{1/2}$. To acquire a good spectrum for this state, an ablation-laser intensity ~ 10 mJ/pulse was used, much higher than the typical intensity of a few mJ/pulse we used. As depicted in the inset of Fig. 1(a), a series of peaks related to the photodetachment channel from $^2\Pi_{1/2}$ to $(^3\Sigma_g^-) 0_g^+$ were observed. The energy level of the $^2\Pi_{1/2}$ state was determined to be $1498(17)$ cm^{-1} above the ground state $^2\Pi_{3/2}$.

For an accurate determination of the electron affinity (EA) of Te_2 , the photoelectron spectrum was further measured near the photodetachment threshold at a photon energy of 16758 cm^{-1} . As displayed in Fig. S2, the full width at half maximum (FWHM) of the EA peak is 9.2 cm^{-1} , which was used to estimate the uncertainty. As a result, the EA value of Te_2 was determined to be $16689.7(92)$ cm^{-1} or $2.0693(11)$ eV, with a significantly improved accuracy compared to the value $1.92(7)$ eV reported by Snodgrass *et al.* previously.²⁵ The uncertainty is mainly due to the rotational

broadening. Several of these peaks can be observed at different photon energies, and the binding energies provided in Table S1 are the most accurate measurement spectra in which a given vibrational peak exhibits the lowest kinetic energy. In addition, the anisotropy parameters (β values) for the observed vibrational peaks in the overview spectrum measured with 480 nm photons are also summarized in Table S1. The angular distributions with β values ranging from -0.4 to -0.9 suggest an (s + d)-wave for the outgoing electron, which is consistent with the detachment from a π -orbital.

The dissociation energy (D_0) of Te_2^- can be obtained by using the following energetic relation:

$$D_0(\text{Te}_2^-) = \text{EA}(\text{Te}_2) - \text{EA}(\text{Te}) + D_0(\text{Te}_2). \quad (1)$$

Having determined $\text{EA}(\text{Te}_2)$ in the present experiment and utilizing the literature values of $1.970861(9)$ eV for $\text{EA}(^{130}\text{Te})$ ⁴⁵ and $2.625(12)$ eV for $D_0(\text{Te}_2)$,⁹ we calculated the value of $D_0(\text{Te}_2^-)$ to be $2.724(12)$ eV. The fundamental vibrational frequency of Te_2^-

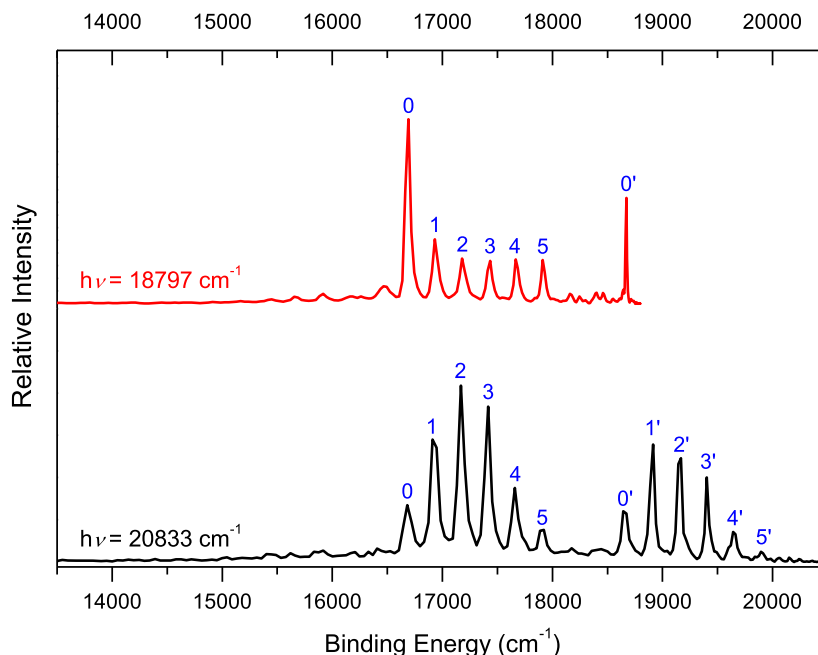


FIG. 2. Comparison of the resonant photoelectron spectrum at 532 nm (18797 cm^{-1} , red curve) with the non-resonant photoelectron spectrum at 480 nm (20833 cm^{-1} , black curve). The weak peaks located before peak 0 are due to the metastable state $^2\Pi_{1/2}$.

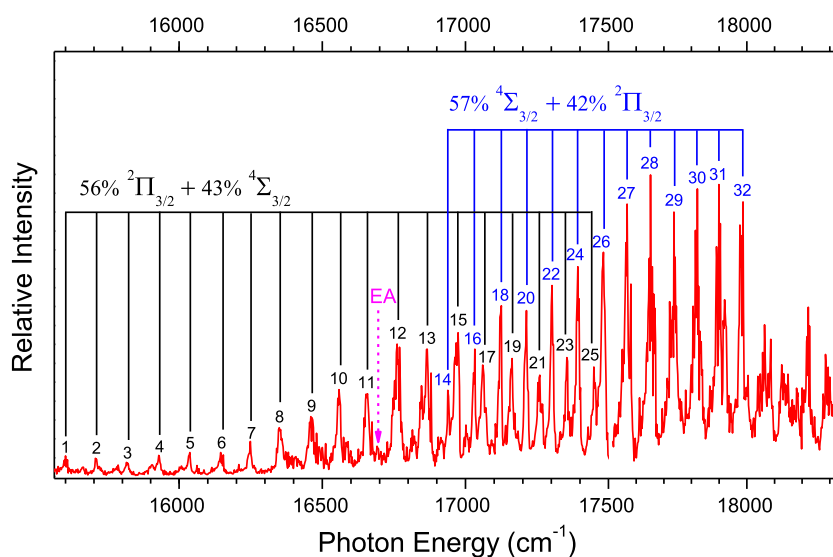


FIG. 3. Photodetachment spectrum of Te_2^- by measuring the total electron yield as a function of photon energy from 15560 to 18350 cm^{-1} using the OPO signal light. The pink dashed arrow indicates the electron affinity of Te_2 or the detachment threshold.

was determined to be $217(13) \text{ cm}^{-1}$ from the spectrum at the photon energy of 16848 cm^{-1} , in which the hot bands were remarkably enhanced through resonance. Refer to Fig. S1 of the supplementary material.

The Franck–Condon (FC) profile in Fig. 1(a) contains the information of the potential curves both for the anionic and for the neutral tellurium dimers. Given the well-known spectroscopic constants of neutral Te_2 from the NIST database,^{22,23,57–59} and the

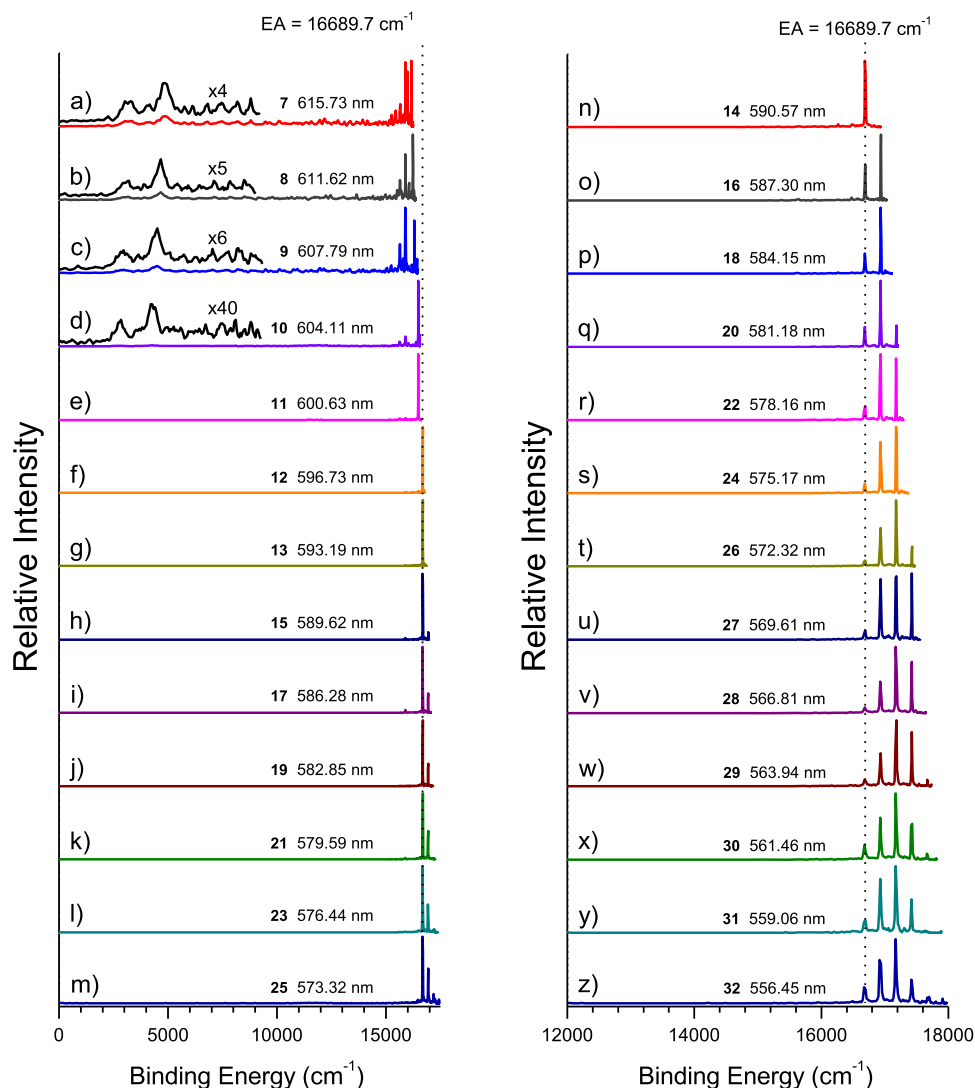


FIG. 4. Resonant photoelectron energy spectra of Te_2^- at the positions of peaks 7–32 in the photodetachment spectrum. Panels (a)–(m) contain resonant photoelectron spectra with different vibrational excited states for the first electronically excited state ($56\% \ ^2\Pi_{3/2} + 43\% \ ^4\Sigma_{3/2}$) of Te_2^- . Below the photodetachment threshold, these weak peaks related to the resonant two-photon transition (black curves) are multiplied by certain factors. Panels (n)–(z) contain resonant photoelectron spectra with different vibrational excited states for the second electronically excited state ($57\% \ ^4\Sigma_{3/2} + 42\% \ ^2\Pi_{3/2}$) of Te_2^- above the photodetachment threshold. The vertical dotted line indicates the EA(Te_2).

determined fundamental vibrational frequency as well as the dissociation energy D_0 of Te_2^- in the present work, the Franck–Condon (FC) simulation for two prominent bands in Fig. 1(a) can be performed by adjusting the equilibrium bond length (r_e) of Te_2^- via the PASCAL program to best reproduce the experimental spectra.^{60,61} The FC simulation has taken into account the Wigner threshold law.⁶² Within the Morse potential, the harmonic vibrational constant ω_e and the dissociation energy D_0 have the following relations:

$$\omega_e = \frac{2\nu_0 D_0}{2D_0 - \nu_0}, \quad (2)$$

$$\omega_e \chi_e = \frac{\omega_e \nu_0}{4D_0}. \quad (3)$$

Here, ν_0 represents the fundamental vibrational frequency, with $\nu_0 = \omega_e - 2\omega_e \chi_e$, where $\omega_e \chi_e$ is the anharmonic constant. As shown in Fig. 1(b), the simulated peak positions and intensities are in excellent agreement with the experimental data, suggesting that the estimated equilibrium bond length r_e , ω_e , and $\omega_e \chi_e$ for the ground state of Te_2^- anions are reasonable. The spectroscopic constants for Te_2^- were determined to be $r_e = 2.669(5) \text{ \AA}$, $\omega_e = 218(13) \text{ cm}^{-1}$, and $\omega_e \chi_e = 0.54(6) \text{ cm}^{-1}$.

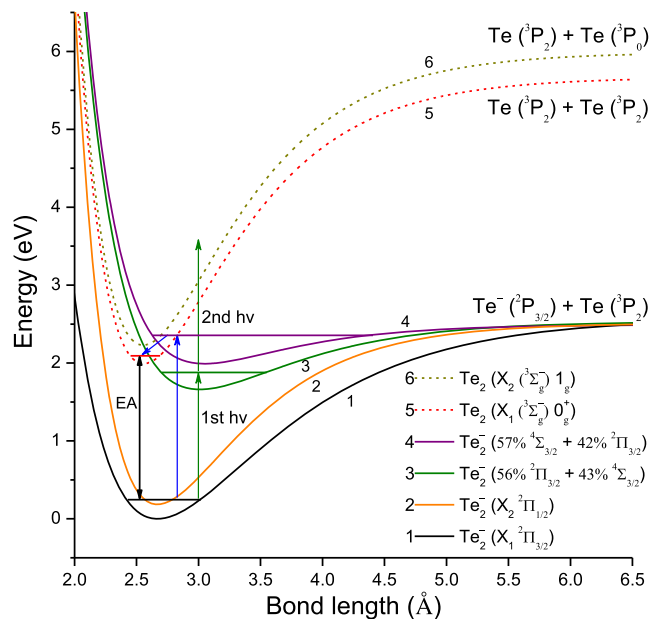


FIG. 5. Schematic potential energy curves for the ground state of Te_2^- ($^2\Pi_{3/2}$), the metastable state of Te_2^- ($^2\Pi_{1/2}$), the two electronically excited states of Te_2^- ($56\% \ ^2\Pi_{3/2} + 43\% \ ^4\Sigma_{3/2}$ and $57\% \ ^4\Sigma_{3/2} + 42\% \ ^2\Pi_{3/2}$), the neutral Te_2 ground state [$(^3\Sigma_g^-)0_g^+$], and the excited state [$(^3\Sigma_g^-)1_g$].

B. Feshbach resonant photodetachment

Normally, the vibrational transition intensities in the photoelectron spectra are governed by the Franck–Condon principle. However, the intensity of the vibrational peaks of Te_2^- appears abnormal at a few specific photon energies. Figure 2 shows the comparison of the photoelectron spectra at $h\nu = 18\,797\text{ cm}^{-1}$ (532 nm) and $h\nu = 20\,833\text{ cm}^{-1}$ (480 nm). Peaks 0 and 0' in the photoelectron spectrum at 532 nm are significantly enhanced. This phenomenon is typically attributed to resonant enhancement. To search for the detailed information for the resonant energy levels of Te_2^- , the resonant photodetachment spectrum was recorded by scanning the detachment laser wavelength across the detachment threshold from 642.67 to 544.96 nm and monitoring the total electron yield. As

shown in Fig. 3, dense sharp peaks were observed and labeled as 1–32 across the detachment threshold. To interpret these sharp peaks, we conducted MRCI calculations for the possible electronic states of Te_2^- . Our calculations predicted that there are two excited states of Te_2^- near its photodetachment threshold. One is situated 1.82 eV above the ground state. This state exhibits significant mixing of $^2\Pi_{3/2}$ and $^4\Sigma_{3/2}$ terms due to the spin–orbital coupling effect. The leading terms of the contributions are 56% $^2\Pi_{3/2}$ and 43% $^4\Sigma_{3/2}$. The other is positioned 2.01 eV above the ground state with a composition of 57% $^4\Sigma_{3/2} + 42\% \ ^2\Pi_{3/2}$. These peaks in Fig. 3 can be grouped into two nearly equally spaced series, which are related to vibrational excitations of the two electronically excited states of Te_2^- ($56\% \ ^2\Pi_{3/2} + 43\% \ ^4\Sigma_{3/2}$ and $57\% \ ^4\Sigma_{3/2} + 42\% \ ^2\Pi_{3/2}$). The wavelengths, photon energies, and energy shifts relative to peak 1 of these vibrational Feshbach resonances are summarized in Table S2.

We assigned peak 1 with an energy $1092(17)\text{ cm}^{-1}$ below the photodetachment threshold as the vibrational ground state of the first electronically excited state of Te_2^- ($56\% \ ^2\Pi_{3/2} + 43\% \ ^4\Sigma_{3/2}$) and peak 14 above the photodetachment threshold by $250(11)\text{ cm}^{-1}$ as the vibrational ground state of the second electronically excited state of Te_2^- ($57\% \ ^4\Sigma_{3/2} + 42\% \ ^2\Pi_{3/2}$). The vibrational progressions for these states can be fitted by Eq. (4) to yield $\omega_e = 111.3 \pm 0.5\text{ cm}^{-1}$ and $\omega_e\chi_e = 0.44 \pm 0.03\text{ cm}^{-1}$ for the first electronically excited state and $\omega_e = 94.2 \pm 0.5\text{ cm}^{-1}$ and $\omega_e\chi_e = 0.55 \pm 0.04\text{ cm}^{-1}$ for the second electronically excited state. The vibrational energy E_v of the Morse potential is given by

$$\frac{E_v}{hc} = \omega_e \left(v + \frac{1}{2} \right) - \omega_e \chi_e \left(v + \frac{1}{2} \right)^2. \quad (4)$$

By tuning the detachment laser to the wavelengths corresponding to the resonant peaks (7–32) in Fig. 3, two series of resonantly enhanced photoelectron spectra were obtained, as depicted in Fig. 4. Figures 4(a)–4(e) show the resonant photoelectron spectra below the photodetachment threshold, in which the bands containing a few broad peaks at the low binding energy side are from the resonant two-photon detachment (R2PD): Te_2^- in the ground state was resonantly excited to the first electronically excited state of Te_2^- anion and was then photodetached by a second photon. When the photon energy exceeded the photodetachment threshold, the

TABLE I. Spectroscopic constants of Te_2^- anion and neutral Te_2 ^a.

Electronic state	Experimental energy (cm^{-1})	r_e (Å)	ω_e (cm^{-1})	$\omega_e\chi_e$ (cm^{-1})
Te_2^- $^2\Pi_{3/2}$	0	2.669(5)	218(13)	0.54(6)
Te_2^- $56\% \ ^2\Pi_{3/2} + 43\% \ ^4\Sigma_{3/2}$	15 598(14)	3.01 ^b	111.3(5)	0.44(3)
Te_2^- $57\% \ ^4\Sigma_{3/2} + 42\% \ ^2\Pi_{3/2}$	16 940(6)	3.05 ^b	94.2(5)	0.55(4)
Te_2 $(^3\Sigma_g^-)0_g^+$	0	2.5574	247.07	0.5148(9)
Te_2 $(^3\Sigma_g^-)1_g$	1974.9	2.5530	250.033	0.5155

^aSpectroscopic constants of neutral Te_2 are obtained from the NIST database.^{22,23,57–59}

^bThe equilibrium bond lengths are from quantum chemical calculations.

$0 \leftarrow 0$ peaks of the photoelectron spectra in Figs. 4(f)–4(m) were significantly enhanced, which were contributed by the fast autodetachment through the Feshbach resonance.⁶³ Figures 4(n)–4(z) show the resonance-enhanced photoelectron spectra above the photodetachment threshold associated with the second electronically excited state of Te_2^- ($57\% \ ^4\Sigma_{3/2} + 42\% \ ^2\Pi_{3/2}$). Figure 5 illustrates the principles of the R2PD and the autodetachment via a Feshbach resonance related to the present measurements. The potential energy curves in solid lines are for Te_2^- , while the curves in dashed lines are for Te_2 . When the photon energy is below the EA threshold of Te_2 , two photons are required to photodetach Te_2^- in the R2PD process. The initial photon resonantly excites Te_2^- , and the subsequent photon facilitates the detachment of the excited state. Once the photon energy surpasses the EA threshold of Te_2 , a resonant autodetachment occurs if the photon energy matches the transition to a quasi-bound state of Te_2^- from its ground state. This Feshbach-resonance process is elucidated in Fig. 5 through the representation of blue arrows. The quasi-bound state has a vibrationally excited core, and its vibrational energy is higher than the binding energy of the electron. The quasi-bound electron was then thrown out due to the vibronic coupling in the autodetachment process.

Table I summarizes the spectroscopic constants of the ground state ($^2\Pi_{3/2}$) and the two electronically excited states ($56\% \ ^2\Pi_{3/2} + 43\% \ ^4\Sigma_{3/2}$ and $57\% \ ^4\Sigma_{3/2} + 42\% \ ^2\Pi_{3/2}$) of Te_2^- determined in the present work, along with the corresponding spectroscopic constants of two splitting electronic states ($^3\Sigma_g^-$) 0_g^+ and ($^3\Sigma_g^-$) 1_g of the neutral counterpart obtained from the NIST database.^{22,23,57–59}

IV. CONCLUSIONS

In conclusion, we investigated both non-resonant and high-resolution resonant photoelectron spectra of cryogenically cooled Te_2^- via the slow-electron velocity-map imaging (SEVI) method. The electron affinity of Te_2 was measured as $16\,689.7(92) \text{ cm}^{-1}$ or $2.0693(11) \text{ eV}$. Two Feshbach resonant states were observed via the photodetachment spectrum of Te_2^- , and their vibrational ground states were located at $1092(17) \text{ cm}^{-1}$ below the photodetachment threshold and $250(11) \text{ cm}^{-1}$ above the photodetachment threshold. The acquired series of resonant photoelectron spectra at the vibrational Feshbach resonances enhance our understanding of the autodetachment dynamics in Te_2^- . Furthermore, our experiment yielded spectroscopic constants for the ground state and two electronically excited states of the Te_2^- anion, serving as a valuable benchmark for further theoretic investigations of the tellurium dimer anion.

SUPPLEMENTARY MATERIAL

The supplementary material contains a summary of all the observed vibrational peaks and their corresponding assignments in the non-resonant photoelectron at 480 nm , along with the anisotropy parameters (β values) for the observed vibrational peaks; a summary of the resonances observed in the photodetachment spectrum of Te_2^- , the corresponding wavelengths, photon energies, and energy shifts with respect to peak 1; and the photoelectron

kinetic energy spectrum measured near the photodetachment threshold at a photon energy of $16\,758 \text{ cm}^{-1}$.

ACKNOWLEDGMENTS

This work was supported by the National Natural Science Foundation of China (NSFC) (Grant Nos. 12374244 and 11974199), the National Key R & D Program of China (Grant No. 2018YFA0306504), and Postdoctoral Fellowship Program of CPSF (Grant No. GZC20231367).

AUTHOR DECLARATIONS

Conflict of Interest

The authors have no conflicts to disclose.

Author Contributions

Shuaiting Yan: Writing – original draft (lead). **Rui Zhang:** Writing – original draft (supporting). **Yuzhu Lu:** Writing – original draft (supporting). **Chuangang Ning:** Writing – review & editing (lead).

DATA AVAILABILITY

The data that support the findings of this study are available within the article and its supplementary material.

REFERENCES

- 1 D. Reinen and G.-G. Lindner, *Chem. Soc. Rev.* **28**, 75 (1999).
- 2 K. D. Setzer and E. H. Fink, *J. Mol. Spectrosc.* **304**, 28 (2014).
- 3 D. G. Streets and J. Berkowitz, *J. Electron Spectrosc. Relat. Phenom.* **9**, 269 (1976).
- 4 S. Tiwari, P. Tandon, and K. N. Uttam, *J. Spectrosc.* **2013**, 956581.
- 5 C. Wei, X. Zhang, D. Ding, and B. Yan, *Chin. Phys. B* **25**, 013102 (2016).
- 6 C. Heinemann, W. Koch, G.-G. Lindner, D. Reinen, and P.-O. Widmark, *Phys. Rev. A* **54**, 1979 (1996).
- 7 Q. Dong, K. Zhang, J. Chen, W. Chen, X. Feng, X. Li, Z. He, J. Qiu, and S. Zhou, *Ceram. Int.* **49**, 22313 (2023).
- 8 S. Sinnecker and W. Koch, *Phys. Chem. Chem. Phys.* **2**, 2219 (2000).
- 9 J. Vergès, C. Effantin, O. Babaky, J. d'Incan, S. J. Prosser, and R. F. Barrow, *Phys. Scr.* **25**, 338 (1982).
- 10 A. Topouzkhanian, O. Babaky, J. Vergès, R. Willers, and B. Wellegehausen, *J. Mol. Spectrosc.* **113**, 39 (1985).
- 11 A. M. Polo, A. Pardo, J. J. Camacho, and J. M. L. Poyato, *Chem. Phys. Lett.* **349**, 235 (2001).
- 12 J. Vergès, J. d'Incan, C. Effantin, D. J. Greenwood, and R. F. Barrow, *J. Phys. B: At. Mol. Phys.* **12**, L301 (1979).
- 13 G.-G. Lindner, K. Witke, H. Schlaich, and D. Reinen, *Inorg. Chim. Acta* **252**, 39 (1996).
- 14 F. Ahmed and E. R. Nixon, *J. Mol. Spectrosc.* **87**, 101 (1981).
- 15 R. Larciprete and M. Stuke, *Appl. Phys. B* **41**, 213 (1986).
- 16 L. R. Maxwell and V. M. Mosley, *Phys. Rev.* **57**, 21 (1940).
- 17 J. Berkowitz and W. A. Chupka, *J. Chem. Phys.* **50**, 4245 (1969).
- 18 K. K. Yee and R. F. Barrow, *J. Chem. Soc., Faraday Trans. 2* **68**, 1397 (1972).
- 19 R. F. Barrow and K. K. Yee, *Acta Phys. Acad. Sci. Hung.* **35**, 239 (1974).
- 20 S. Li, R. J. Van Zee, and W. Weltner, Jr., *J. Chem. Phys.* **99**, 762 (1993).
- 21 J. Berkowitz, *J. Chem. Phys.* **62**, 4074 (1975).
- 22 T. J. Stone and R. F. Barrow, *Can. J. Phys.* **53**, 1976 (1975).

- ²³V. E. Bondybey and J. H. English, *J. Chem. Phys.* **72**, 6479 (1980).
- ²⁴C. Effantin, J. D'Arcan, J. Vergès, M. T. Macpherson, and R. F. Barrow, *Chem. Phys. Lett.* **70**, 560 (1980).
- ²⁵J. T. Snodgrass, J. V. Coe, K. M. McHugh, C. B. Freidhoff, and K. H. Bowen, *J. Phys. Chem.* **93**, 1249 (1989).
- ²⁶D. J. Meschi and A. W. Searcy, *J. Chem. Phys.* **51**, 5134 (2003).
- ²⁷P. Hassanzadeh, C. Thompson, and L. Andrews, *J. Phys. Chem.* **96**, 8246 (1992).
- ²⁸K. F. Willey, P. Y. Cheng, T. G. Taylor, M. B. Bishop, and M. A. Duncan, *J. Phys. Chem.* **94**, 1544 (1990).
- ²⁹K. Nagaya, A. Oohata, I. Yamamoto, and M. Yao, *J. Non-Cryst. Solids* **312–314**, 337 (2002).
- ³⁰B. C. Pan, *Phys. Rev. B* **65**, 085407 (2002).
- ³¹H. H. Abdallah, *Can. J. Phys.* **98**, 57 (2020).
- ³²V. S. Ghemud, H. A. S. Gol, and A. Kshirsagar, *J. Nanopart. Res.* **20**, 177 (2018).
- ³³K. Balasubramanian and C. Ravimohan, *J. Mol. Spectrosc.* **126**, 220 (1987).
- ³⁴A. Zaitsevskii, R. Ferber, and C. Teichtel, *Phys. Rev. A* **63**, 042511 (2001).
- ³⁵C. Heinemann, W. Koch, and P. O. Widmark, *Mol. Phys.* **92**, 463 (1997).
- ³⁶I. León, Z. Yang, H.-T. Liu, and L.-S. Wang, *Rev. Sci. Instrum.* **85**, 083106 (2014).
- ³⁷Z. Luo, X. Chen, J. Li, and C. Ning, *Phys. Rev. A* **93**, 020501 (2016).
- ³⁸D. M. Neumark, *J. Phys. Chem. A* **112**, 13287 (2008).
- ³⁹A. Osterwalder, M. J. Nee, J. Zhou, and D. M. Neumark, *J. Chem. Phys.* **121**, 6317 (2004).
- ⁴⁰M. L. Weichman and D. M. Neumark, *Annu. Rev. Phys. Chem.* **69**, 101 (2018).
- ⁴¹R. Zhang, Y. Lu, R. Tang, and C. Ning, *J. Chem. Phys.* **158**, 084303 (2023).
- ⁴²X. Chen and C. Ning, *Phys. Rev. A* **93**, 052508 (2016).
- ⁴³R. Tang, X. Fu, and C. Ning, *J. Chem. Phys.* **149**, 134304 (2018).
- ⁴⁴C. Ning and Y. Lu, *J. Phys. Chem. Ref. Data* **51**, 021502 (2022).
- ⁴⁵S. Yan, Y. Lu, R. Zhang, and C. Ning, *Chin. J. Chem. Phys.* **37**, 1 (2024).
- ⁴⁶W. C. Wiley and I. H. McLaren, *Rev. Sci. Instrum.* **26**, 1150 (1955).
- ⁴⁷D. W. Chandler and P. L. Houston, *J. Chem. Phys.* **87**, 1445 (1987).
- ⁴⁸B. Dick, *Phys. Chem. Chem. Phys.* **16**, 570 (2014).
- ⁴⁹B. Dick, *Phys. Chem. Chem. Phys.* **21**, 19499 (2019).
- ⁵⁰R. Tang, X. Fu, Y. Lu, and C. Ning, *J. Chem. Phys.* **152**, 114303 (2020).
- ⁵¹R. Tang, R. Si, Z. Fei, X. Fu, Y. Lu, T. Brage, H. Liu, C. Chen, and C. Ning, *Phys. Rev. A* **103**, 042817 (2021).
- ⁵²H.-J. Werner, P. J. Knowles, G. Knizia, F. R. Manby, and M. Schütz, *Wiley Interdiscip. Rev.: Comput. Mol. Sci.* **2**, 242 (2012).
- ⁵³D. Feller, *J. Comput. Chem.* **17**, 1571 (1996).
- ⁵⁴K. A. Peterson, D. Figgen, E. Goll, H. Stoll, and M. Dolg, *J. Chem. Phys.* **119**, 11113 (2003).
- ⁵⁵B. P. Pritchard, D. Altarawy, B. Didier, T. D. Gibson, and T. L. Windus, *J. Chem. Inf. Model.* **59**, 4814 (2019).
- ⁵⁶K. L. Schuchardt, B. T. Didier, T. Elsethagen, L. Sun, V. Gurumoorthi, J. Chase, J. Li, and T. L. Windus, *J. Chem. Inf. Model.* **47**, 1045 (2007).
- ⁵⁷P. J. Linstrom and E. W. G. Mallard, *NIST Chemistry WebBook, NIST Standard Reference Database Number 69*, National Institute of Standards and Technology, Gaithersburg, MD, p. 20899 (retrieved 6 December 2023).
- ⁵⁸S. Smoes, F. Mandy, A. V. Auwera-Mahieu, and J. Drowart, *Bull. Soc. Chim. Belg.* **81**, 45 (1972).
- ⁵⁹K. P. Huber and G. Herzberg, *Molecular Spectra and Molecular Structure: IV. Constants of Diatomic Molecules* (Van Nostrand, New York, 1979), p. 716.
- ⁶⁰K. M. Ervin and W. C. Lineberger, *PESCAL, Fortran program*, 2010.
- ⁶¹M. L. Polak, G. Gerber, J. Ho, and W. C. Lineberger, *J. Chem. Phys.* **97**, 8990 (1992).
- ⁶²E. P. Wigner, *Phys. Rev.* **73**, 1002 (1948).
- ⁶³D. H. Kang, S. An, and S. K. Kim, *Phys. Rev. Lett.* **125**, 093001 (2020).